Hybrid functionals applied to extended systems

2008 J. Phys.: Condens. Matter 20 064201

(http://iopscience.iop.org/0953-8984/20/6/064201)

J. Phys.: Condens. Matter **20** (2008) 064201 (9pp) doi:10.1088/0953-8984/20/6/064201

Hybrid functionals applied to extended systems

M Marsman, J Paier, A Stroppa and G Kresse

Faculty of Physics, Universität Wien, and Center for Computational Materials Science, Sensengasse 8/12, A-1090 Vienna, Austria

Received 29 October 2007, in final form 5 December 2007
Published 24 January 2008
Online at stacks.iop.org/JPhysCM/20/064201

Abstract

We present an overview of the description of structural, thermochemical, and electronic properties of extended systems using several well known hybrid Hartree–Fock/density-functional-theory functionals (PBE0, HSE03, and B3LYP). In addition we address a few aspects of the evaluation of the Hartree–Fock exchange interactions in reciprocal space, relevant to all methods that employ a plane wave basis set and periodic boundary conditions.

(Some figures in this article are in colour only in the electronic version)

1. Introduction

Kohn–Sham density functional theory (DFT) has proven to be a very powerful tool for the quantitative prediction of materials properties, both in computational solid state physics and in quantum chemistry. In its most commonly applied approximations to the electronic exchange and correlation, i.e. in the local density approximation (LDA) and the semilocal generalized gradient approximation (GGA), DFT is highly efficient and surprisingly accurate. Still, though, present local and semilocal functionals show significant errors, for instance, in the energetics of small molecules and in the description of the band gaps of extended systems.

Hybrid functionals, i.e. exchange–correlation functionals that admix a certain amount of Hartree–Fock (HF) exchange to (a part of) a local or semilocal density functional, have been shown to remedy several deficiencies of the latter. Most notably, HF/DFT hybrid functionals are known to present an improved description of the thermochemistry of molecular systems [1–4]. Due to the large computational effort required to evaluate the Hartree–Fock exchange under periodic boundary conditions, however, HF/DFT hybrid schemes have rarely been applied to periodic systems, and comprehensive systematic studies of the HF/DFT description of extended systems were largely lacking until recently. The past several years have seen a change, with a number of papers published providing a detailed evaluation of the description of structural, thermochemical, and electronic properties of extended systems using the PBE0, HSE03, and B3LYP HF/DFT hybrid functionals [5–8].

This contribution presents a summary of the main characteristics of the aforementioned hybrid functionals applied to extended systems. As such it recapitulates the results presented in [7] and [8] (and references therein), on lattice parameters, bulk moduli, atomization energies, heats of formation, band gaps, and band widths for a selection of archetypical metallic, semiconducting and ionic solid state systems. Additionally, we discuss the results of hybrid functional calculations on transition metal monoxides (TMOs) and the adsorption of carbon monoxide on d-metal surfaces.

The remainder of this paper is organized as follows: in section 2 the expressions for the PBE0, HSE03, and B3LYP exchange–correlation energy are given. Section 3 deals with several computational aspects of the Hartree–Fock exchange interaction in reciprocal space, relevant to methods that use a plane wave basis set and periodic boundary conditions. Results are presented in section 4, conclusions in section 5.

2. Theory

Under periodic boundary conditions, the nonlocal Hartree–Fock exchange energy $E_{\mathrm{X}}^{\mathrm{HF}}$ (in real space) can be written as

$$E_{\mathrm{X}}^{\mathrm{HF}} = -\frac{e^2}{2}\sum_{\mathbf{k}n,\mathbf{q}m} 2w_{\mathbf{k}} f_{\mathbf{k}n} \times w_{\mathbf{q}} f_{\mathbf{q}m} \times \int\int \mathrm{d}^3\mathbf{r}\,\mathrm{d}^3\mathbf{r}' \frac{\phi^*_{\mathbf{k}n}(\mathbf{r})\phi_{\mathbf{q}m}(\mathbf{r})\phi^*_{\mathbf{q}m}(\mathbf{r}')\phi_{\mathbf{k}n}(\mathbf{r}')}{|\mathbf{r}-\mathbf{r}'|}, \quad (1)$$

where $\{\phi_{\mathbf{k}n}(\mathbf{r})\}$ is the set of one-electron Bloch states of the system, and $\{f_{\mathbf{k}n}\}$ the corresponding set of (possibly fractional) occupational numbers. The sums over $\mathbf{k}$ and $\mathbf{q}$ run over all k-points chosen to sample the Brillouin zone (BZ), whereas the sums over m and n are performed over all bands at these

k-points. The k-point weights w_k sum to one, and the factor 2 accounts for the fact that we consider a spin degenerated system.

2.1. PBE0

The PBE0 hybrid functional [2, 3] is constructed by mixing 25% of Hartree–Fock exchange to 75% of the well known PBE exchange [9]. The electronic correlation is represented by the corresponding part of the PBE density functional. Thus, the resulting exchange–correlation energy expression takes the following simple form:

$$E_{\mathrm{xc}}^{\mathrm{PBE0}} = \tfrac{1}{4}E_{\mathrm{X}}^{\mathrm{HF}} + \tfrac{3}{4}E_{\mathrm{X}}^{\mathrm{PBE}} + E_{\mathrm{c}}^{\mathrm{PBE}}, \tag{2}$$

where $E_{\mathrm{X}}^{\mathrm{PBE}}$ and $E_{\mathrm{c}}^{\mathrm{PBE}}$ denote the PBE exchange and correlation energies, respectively. The 1:3 mixing ratio of Hartree–Fock to PBE exchange is based on a conceptual model devised by Ernzerhof and co-workers [10–12]. Hybrid functionals based on their work are often called 'parameter-free' or non-empirical, since the amount of Hartree–Fock exchange to be admixed is not determined by a fit to experimental data.

2.2. HSE03

Depending on the decay of the Hartree–Fock exchange interactions with distance, the evaluation of $E_{\mathrm{X}}^{\mathrm{HF}}$ (equation (1)) may be computationally very demanding. The decay is highly system dependent and may range from a few to up to hundreds of Ångstroms. To avoid the calculation of expensive integrals over slowly decaying exchange interactions, Heyd *et al* [13] proposed to replace the long-range part of the Hartree–Fock exchange in the PBE0 HF/DFT hybrid by a corresponding density functional counterpart. The resulting expression for the exchange–correlation energy (HSE03) is given by

$$E_{\mathrm{xc}}^{\mathrm{HSE03}} = \tfrac{1}{4}E_{\mathrm{X}}^{\mathrm{HF,sr},\mu} + \tfrac{3}{4}E_{\mathrm{X}}^{\mathrm{PBE,sr},\mu} + E_{\mathrm{X}}^{\mathrm{PBE,lr},\mu} + E_{\mathrm{c}}^{\mathrm{PBE}}, \tag{3}$$

where (sr) and (lr) denote the short- and long-range parts of the respective exchange interactions (HF or PBE exchange). The separation of the exchange interactions into short- and long-range parts is accomplished through a decomposition of the Coulomb kernel

$$\frac{1}{r} = S_\mu(r) + L_\mu(r) = \frac{\mathrm{erfc}(\mu r)}{r} + \frac{\mathrm{erf}(\mu r)}{r}, \tag{4}$$

where $r = |\mathbf{r} - \mathbf{r}'|$, and μ is the parameter that defines the range separation. μ is related to a characteristic distance, $(2/\mu)$, at which the short-range interactions become negligible. Thus $E_{\mathrm{X}}^{\mathrm{HF,sr},\mu}$ is given by equation (1), provided one replaces the Coulomb kernel by $S_\mu(r)$. The short- and long-range parts of the PBE exchange energy are derived using the same decomposition (equation (4)) [13]. Empirically, it was shown that the optimum range-separation parameter μ is between 0.2 and 0.3 Å^{-1} [13, 14]. Consequently, the HSE03 functional is a semiempirical functional. In general, one finds that the results using HSE03 are very similar to those obtained using the PBE0.

2.3. B3LYP

The B3LYP functional [15, 16] follows the 'formal structure' of the hybrid functionals proposed by Becke [17]. The exchange energy is given by

$$E_{\mathrm{X}}^{\mathrm{B3LYP}} = 0.8E_{\mathrm{X}}^{\mathrm{LDA}} + 0.2E_{\mathrm{X}}^{\mathrm{HF}} + 0.72\Delta E_{\mathrm{X}}^{\mathrm{B88}}, \tag{5}$$

where E_X^{LDA} and $\Delta E_{\mathrm{X}}^{\mathrm{B88}}$ are the LDA exchange and the gradient corrections to the Becke88 exchange [18], respectively.

The B3LYP correlation energy is defined as

$$E_{\mathrm{C}}^{\mathrm{B3LYP}} = 0.19E_{\mathrm{C}}^{\mathrm{VWN3}} + 0.81E_{\mathrm{C}}^{\mathrm{LYP}}, \tag{6}$$

where $E_{\mathrm{C}}^{\mathrm{VWN3}}$ and $E_{\mathrm{C}}^{\mathrm{LYP}}$ denote the correlation energy from the Vosko–Wilk–Nusair III [19] and the Lee–Yang–Parr [20] correlation functionals, respectively.

The B3LYP functional is a semiempirical functional. The coefficients in equations (5) and (6) are determined by a least square fit to atomization energies, electron and proton affinities, and the ionization potentials of the atomic species and molecules in Pople's G2 test set.

3. Computational aspects

In this section we address a few aspects of the evaluation of the Hartree–Fock exchange interactions in reciprocal space, i.e. relevant to all methods that employ a plane wave basis set and periodic boundary conditions. For a detailed description of the HF exchange formalism within the projector-augmented-wave (PAW) method [21] and its implementation in the Vienna *ab initio* simulation package (VASP) [22, 23], we refer to [4] and [7] (and references therein).

3.1. Scaling

To illustrate how to best evaluate equation (1) we first define the overlap density between two Bloch states $a = \mathbf{k}n$ and $b = \mathbf{q}m$ as

$$n_{ab}(\mathbf{r}) = \phi_a^*(\mathbf{r})\phi_b(\mathbf{r}). \tag{7}$$

and the two-orbital exchange potential

$$V_{ab}(\mathbf{r}) = \int \frac{n_{ab}^*(\mathbf{r}')}{|\mathbf{r} - \mathbf{r}'|}\,\mathrm{d}\mathbf{r}'. \tag{8}$$

Note that $n_{ab}(\mathbf{r})$ and $V_{ab}(\mathbf{r})$ are not cell periodic and possess a Bloch wavevector $\mathbf{Q} = \mathbf{q} - \mathbf{k}$. The potential can be conveniently calculated in reciprocal space,

$$V_{ab}(\mathbf{G}) = 4\pi e^2 \frac{n_{ab}(\mathbf{G})}{|\mathbf{G} + \mathbf{q} - \mathbf{k}|^2}, \tag{9}$$

where $n_{ab}(\mathbf{G})$ is the Fourier transform of the cell-periodic part of the overlap density $n_{ab}(\mathbf{r})$. Within a plane wave basis set the latter is easily obtained by means of a fast Fourier transform (FFT$\{n_{ab}(\mathbf{r})\} \rightarrow n_{ab}(\mathbf{G})$). A second FFT yields the cell-periodic part of $V_{ab}(\mathbf{r})$, the two-orbital exchange potential in real space (FFT$\{V_{ab}(\mathbf{G})\} \rightarrow V_{ab}(\mathbf{r})$). Finally, the integral

$$\int \phi_a(\mathbf{r})V_{ab}(\mathbf{r})\phi_b^*(\mathbf{r})\,\mathrm{d}\mathbf{r} \tag{10}$$

is evaluated in real space.

Basically, the above sketches how the explicit convolutions in equation (1) may be avoided at the cost of performing two FFTs. The cost of performing an FFT scales as $N_{\mathrm{FFT}} \ln N_{\mathrm{FFT}}$, where N_{FFT} is the number of points in the FFT grid.

The overall computational cost of evaluating equation (1) is proportional to

$$(N_{\mathrm{bands}} \times N_k)^2 N_{\mathrm{FFT}} \ln N_{\mathrm{FFT}}, \tag{11}$$

where N_k is the number of k-points that sample the first Brillouin zone and N_{bands} is the number of bands at each k-point. The quantities N_{FFT}, N_{bands}, and N_k scale in the following manner with increasing system size (given by the number of atoms in the system, N_{atoms}): $N_{\mathrm{FFT}} \ln N_{\mathrm{FFT}} \propto N_{\mathrm{atoms}}$, $N_{\mathrm{bands}} \propto N_{\mathrm{atoms}}$, and $N_k \propto 1/N_{\mathrm{atoms}}$. Thus, the computational cost for the evaluation of the HF exchange energy scales linearly with the number of atoms ($\propto N_{\mathrm{atoms}}$). One should beware though that this relation breaks down as soon as $N_k = 1$ is reached (e.g. large supercells, molecule in a box), i.e., as soon as N_k cannot be reduced any more upon an increase in system size. For $N_k = 1$ the computational cost scales cubically with the number of atoms ($\propto N_{\mathrm{atoms}}^3$).

3.2. Downsampling

As mentioned in section 2.2, the computational advantage of the HSE03 functional over the PBE0 stems from the elimination of the long-range part of the HF exchange, which leads to a reduction of the domain (in real space) over which the HF exchange integrals have to be evaluated. When the HF exchange is evaluated in reciprocal space, as sketched in section 3.1, the reduction in the computational requirements associated with the HSE03 scheme is of a different form: within a bandstructure picture, the increased locality of the HSE03 HF exchange interactions allows us to evaluate the short-range HF operator on a less dense k-point grid than would be needed to accurately capture the features of the full HF operator. As was shown in [7], this may be exploited in the following manner.

The short-range part of the HF exchange is given by (see section 2.2 and compare to equation (1))

$$E_{\mathrm{X}}^{\mathrm{HF,sr},\mu} = -\frac{e^2}{2} \sum_{\mathbf{k}n,\mathbf{q}m} 2w_{\mathbf{k}} f_{\mathbf{k}n} \times w_{\mathbf{q}} f_{\mathbf{q}m} \times \int\int \mathrm{d}^3\mathbf{r}\, \mathrm{d}^3\mathbf{r}' \frac{\mathrm{erfc}(\mu|\mathbf{r}-\mathbf{r}'|)}{|\mathbf{r}-\mathbf{r}'|} \times \phi^*_{\mathbf{k}n}(\mathbf{r})\phi_{\mathbf{q}m}(\mathbf{r})\phi^*_{\mathbf{q}m}(\mathbf{r}')\phi_{\mathbf{k}n}(\mathbf{r}'), \tag{12}$$

and the corresponding nonlocal short-range HF exchange potential by

$$V_{\mathrm{X}}^{\mathrm{HF,sr},\mu}(\mathbf{r},\mathbf{r}') = -e^2 \sum_{\mathbf{q}m} w_{\mathbf{q}} f_{\mathbf{q}m} \times \mathrm{e}^{\mathrm{i}\mathbf{q}\cdot\mathbf{r}} u_{\mathbf{q}m}(\mathbf{r}) \frac{\mathrm{erfc}(\mu|\mathbf{r}-\mathbf{r}'|)}{|\mathbf{r}-\mathbf{r}'|} u^*_{\mathbf{q}m}(\mathbf{r}')\, \mathrm{e}^{-\mathrm{i}\mathbf{q}\cdot\mathbf{r}'}, \tag{13}$$

where $u_{\mathbf{q}m}(\mathbf{r})$ is the cell-periodic part of the Bloch state $\phi_{\mathbf{q}m}(\mathbf{r})$. As mentioned above, due to the accelerated decay of the kernel $\mathrm{erfc}(\mu|\mathbf{r}-\mathbf{r}'|)/|\mathbf{r}-\mathbf{r}'|$, the short-range HF exchange potential can in most cases be represented on a coarser mesh of k-points in the Brillouin zone than the other contributions to the Hamiltonian. Hence, the sum over $\mathbf{q}$ in equation (13) can be restricted to a subset $\{\mathbf{q}\}$ of the full $(N_1 \times N_2 \times N_3)$ k-point set $\{\mathbf{k}\}$, for which the following holds:

$$\{\mathbf{q}\} = \left\{ \mathbf{k} + \sum_{i=1}^{3} \frac{m_i C_i}{N_i} \mathbf{b}_i \,|\, m_i = 0, \ldots, \frac{N_i}{C_i} - 1 \right\}, \tag{14}$$

where C_i is an integer 'grid reduction factor' along reciprocal lattice direction $\mathbf{b}_i$. This reduces the computational workload by a factor $C_1C_2C_3$ (as can be easily seen from equation (11)).

The above is illustrated by figure 1 depicting the dependence of the PBE0 and HSE03 HF exchange energy of fcc Al on the mesh of k-points ($n_{\mathrm{q}} \times n_{\mathrm{q}} \times n_{\mathrm{q}}$) used to represent the HF exchange potential (the 'downsampled' grid $\{\mathbf{q}\}$). A grid of $(24 \times 24 \times 24)$ k-points was used to represent the wavefunctions on the 'full' grid $\{\mathbf{k}\}$. The points $n_{\mathrm{q}} = 4$, 6, 8, 12, and 24 correspond to grid reduction factors of $C_{1,2,3} = 6$, 4, 3, 2, and 1, respectively.

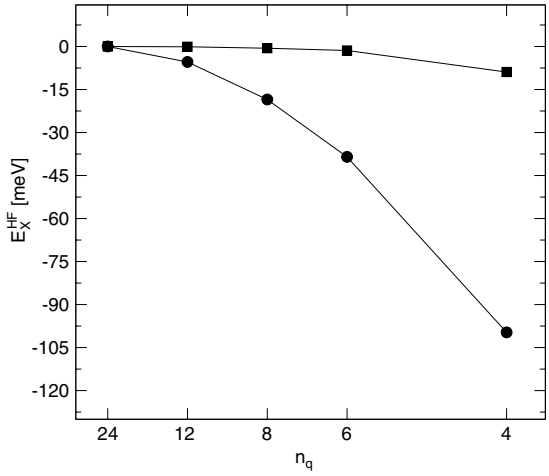

Figure 1. Dependence of the PBE0 (circles) and HSE03 (squares) HF exchange energy of fcc Al on the 'downsampled' $\{\mathbf{q}\}$ mesh ($n_{\mathrm{q}} \times n_{\mathrm{q}} \times n_{\mathrm{q}}$) used to represent the nonlocal HF exchange potential. A $(24 \times 24 \times 24)$ 'full' grid $\{\mathbf{k}\}$ was used to represent the wavefunctions.

As can be seen in figure 1, the reduction in the range of the HF exchange interaction in the HSE03 functional clearly shows up in its $\{\mathbf{q}\}$-mesh representability. The HSE03 HF exchange energy is converged to 1 meV for a $(6 \times 6 \times 6)$ $\{\mathbf{q}\}$-space representation of the HF potential, whereas the PBE0 HF exchange energy still changes by roughly 5 meV, when going from a $(24 \times 24 \times 24)$ to a $(12 \times 12 \times 12)$ $\{\mathbf{q}\}$-sampling and by almost 40 meV when going to a $(6 \times 6 \times 6)$ $\{\mathbf{q}\}$-mesh.

3.3. Accuracy

Our implementation of HF/DFT hybrid functionals within the PAW method was extensively benchmarked against Gaussian type orbital (GTO) local basis set calculations with `GAUSSIAN03` [15]. This is illustrated in figure 2 showing the deviation of the PAW PBE and PBE0 atomization energies

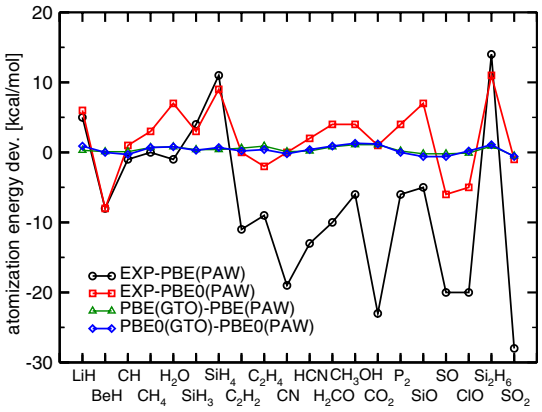

Figure 2. Deviations of the PAW PBE and PBE0 atomization energies with respect to experiment (circles and squares) and GTO calculations (triangles and diamonds), for a subset of Pople's G2-1 test set of small molecules.

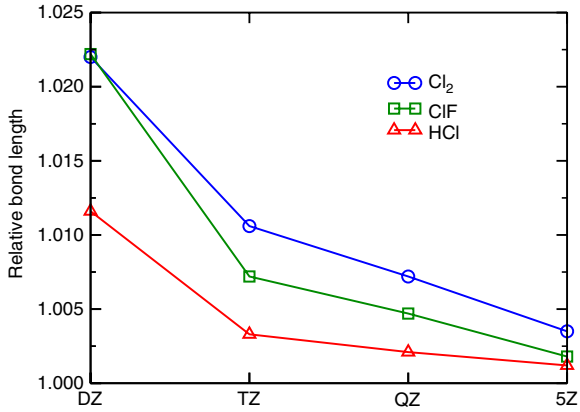

Figure 3. Relative bond lengths of Cl_2, ClF, and HCl obtained with various GTO basis sets (aug-cc-pVXZ (X = D, T, Q, 5)), specified with respect to the PAW PBE result.

with respect to experiment and GTO calculations, for a subset of Pople's G2-1 test set of small molecules (see [4] and references therein).

As can be seen, the agreement between the PAW and GTO atomization energies is excellent, for both PBE (triangles) and PBE0 (diamonds). The mean absolute deviation (MAE) between the PAW PBE and PBE0 atomization energies and the GTO results for the complete G2-1 test set is 0.46 kcal mol^{-1} and 0.49 kcal mol^{-1}, respectively [4]. Furthermore, the deviation between the PAW and GTO atomization energies remains $<$1.5 kcal mol^{-1} for all molecules in the G2-1 set. The level of agreement between plane wave and local basis set calculations is indeed excellent, especially in comparison to the deviations of the PBE and PBE0 atomization energies with respect to experiment (circles and squares in figure 2, respectively).

Comparable benchmarks for the structural parameters of the molecules in the G2-1 test set yield a similar level of agreement between PAW and GTO results [4]. Beware, however, that this kind of quantitative agreement between PAW and GTO calculations is only reached when both are well converged with respect to their respective basis sets. The latter is demonstrated in figure 3, depicting the relative PBE bond lengths of Cl_2, ClF, and HCl, obtained with increasing GTO basis sets (aug-cc-pVXZ (X = D, T, Q, 5)), with respect to well converged PAW results (a (13 × 14 × 15) Å^3 supercell, 1000 eV basis set kinetic energy cut-off).

It is clear that the aug-cc-pVQZ basis sets do not yet yield converged results. Especially for Cl_2, an appreciable change in the bond length is observed when going from an aug-cc-pVQZ to an aug-cc-pV5Z basis set. In this context, one should note that the aug-cc-pV5Z basis set for Cl contains more than 200 basis functions, and the computational expense of the aug-cc-pV5Z GTO calculations in figure 3 exceeds the cost of the corresponding PAW calculations (the break-even point lies somewhere between the aug-cc-pVQZ and aug-cc-pV5Z basis sets).

4. Applications

This section discusses the results of hybrid functional calculations (PBE0, HSE03, and B3LYP) of structural, thermochemical, and electronic properties of a test set of archetypical metallic (Na, Li, Al, Cu, Rh, Pd, and Ag) semiconducting (Si, GaAs, BP, GaP, SiC GaN, C, BN), and ionic (MgO, NaCl, LiCl, NaF, and LiF) solid state systems (see [7] and [8], and references therein). Furthermore, we present an evaluation of the HSE03 and B3LYP description of the structural and electronic properties of several transition metal monoxides (MnO, FeO, CoO, and NiO), and of HSE03 and PBE0 adsorption energies of CO on d-metal surfaces (Cu(111), Rh(111), and Pt(111)).

4.1. Structural properties

Figures 4 and 5 show the relative errors in the PBE, PBE0, HSE03, and B3LYP lattice constants and bulk moduli with respect to experiment, for the materials in the aforementioned test set. Additionally, tables 1 and 2 list several statistical quantities, the mean error (ME), mean absolute error (MAE), mean relative error (MRE), and mean absolute relative error (MARE), to characterize the overall quality of the results with respect to experiment.

As can be seen from figure 4 and table 1 the PBE functional yields an overestimation of the lattice constants (except for Li and Na). The general agreement between the PBE lattice constants and experiment is quite satisfactory; the largest relative error in the lattice constants amounts to 2.1% (for NaF), and the MRE and MARE to 0.8% and 1.0%, respectively. Since the calculated bulk moduli are quite sensitive to the equilibrium volume at which they are evaluated, an error in the theoretical lattice constant with respect to experiment translates into a comparatively large discrepancy in the bulk modulus. Generally speaking the underestimation of lattice constants shows a one-to-one correspondence with an overestimation of bulk moduli, and vice versa. This is clearly illustrated by figure 5 and table 2.

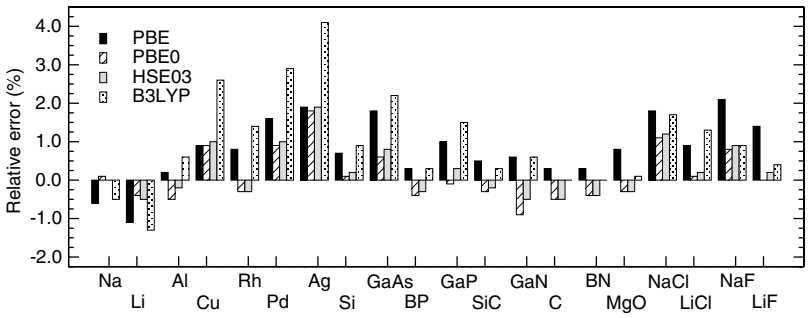

Figure 4. Relative error in the PBE, PBE0, HSE03, and B3LYP lattice constants with respect to experiment.

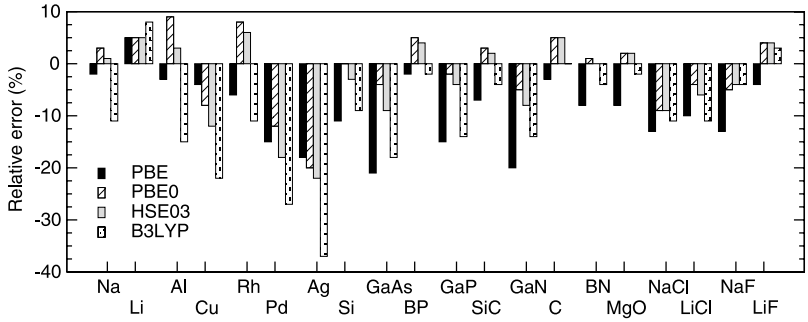

Figure 5. Relative error in the PBE, PBE0, HSE03, and B3LYP bulk moduli with respect to experiment.

Table 1. Mean error ME (Å), mean absolute error MAE (Å), mean relative error MRE, and mean absolute relative error MARE, in the PBE, PBE0, HSE03, and B3LYP lattice constants with respect to experiment.

	PBE	PBE0	HSE03	B3LYP
All solids				
ME	0.038	0.006	0.012	0.046
MAE	0.044	0.022	0.024	0.053
MRE (%)	0.8	0.1	0.2	1.0
MARE (%)	1.0	0.5	0.5	1.2
No metals (Si–LiF)				
ME	0.047	0.002	0.009	0.042
MAE	0.047	0.020	0.022	0.042
MRE (%)	1.0	0.0	0.1	0.8
MARE (%)	1.0	0.4	0.5	0.8

Table 2. Mean error ME (GPa), mean absolute error MAE (GPa), mean relative error MRE, and mean absolute relative error MARE, in the PBE, PBE0, HSE03, and B3LYP bulk moduli with respect to experiment.

	PBE	PBE0	HSE03	B3LYP
All solids				
ME	−12.3	−0.1	−2.6	−13.3
MAE	12.3	7.9	8.6	13.7
MRE (%)	−9.8	−1.2	−3.1	−10.2
MARE (%)	9.4	5.7	6.4	11.4
No metals (Si–LiF)				
ME	−13.3	2.0	0.5	−7.7
MAE	13.3	5.4	5.9	8.1
MRE (%)	−10.4	−0.7	−1.8	−6.8
MARE (%)	10.4	3.8	4.6	7.4

The aforementioned overall overestimation of the lattice constants and corresponding underestimation of the bulk moduli is present in the PBE0 and HSE03 results as well (see figures 4 and 5, and tables 1 and 2), though to a considerably lesser degree (lattice constants: MARE(PBE0) = 0.5%, MARE(HSE03) = 0.5%, compared to MARE(PBE) = 1.0%). The best description of the structural parameters of the materials in the present test set is obtained using the PBE0 hybrid functional, closely followed by the (computationally advantageous) HSE03.

The B3LYP results, on the other hand, present a slight deterioration with respect to those obtained using the PBE density functional (lattice constants: MARE(B3LYP) = 1.2% versus MARE(PBE) = 1.0%). As is evident from figures 4 and 5, this is mostly due to a poor description of the d metals (Cu, Rh, Pd, and Ag).

4.2. Thermochemistry

4.2.1. Atomization energies. Figure 6 shows the relative errors in the PBE, PBE0, HSE03, and B3LYP atomization energies with respect to experiment, for the materials in our test set. The corresponding statistical results (ME, MAE, MRE, and MARE) are given in table 3.

As the latter shows, the overall description of the atomization energies of our set of systems is best at the PBE

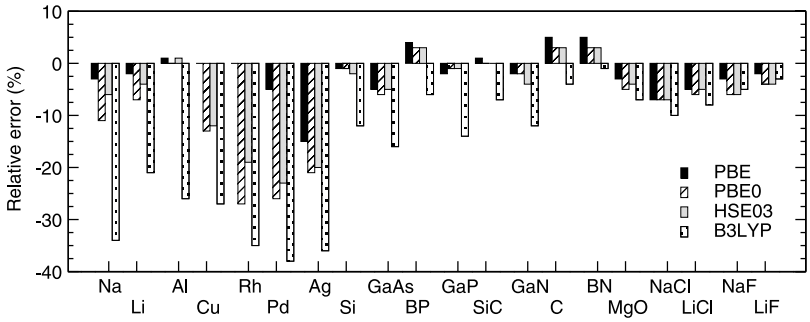

Figure 6. Relative error in the PBE, PBE0, HSE03, and B3LYP atomization energies with respect to experiment.

Table 3. Mean error ME (eV), mean absolute error MAE (eV), mean relative error MRE, and mean absolute relative error MARE, in the PBE, PBE0, HSE03, and B3LYP atomization energies with respect to experiment.

	PBE	PBE0	HSE03	B3LYP
All solids				
ME	−0.045	−0.228	−0.184	−0.590
MAE	0.134	0.286	0.252	0.590
MRE (%)	−1.9	−6.5	−5.1	−17.6
MARE (%)	3.4	7.4	6.3	17.6
No metals (Si–LiF)				
ME	−0.018	−0.067	−0.063	−0.348
MAE	0.156	0.161	0.162	0.348
MRE (%)	−1.2	−2.2	−2.1	−8.0
MARE (%)	3.4	3.6	3.6	8.0

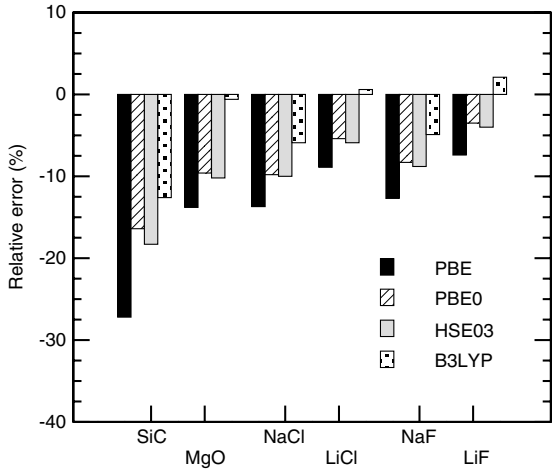

Figure 7. Relative error in the PBE, PBE0, HSE03, and B3LYP heats of formation with respect to experiment.

level (with a MARE of 3.4%, compared to 7.4% and 6.3% and 17.6% (!) for the PBE0, HSE03, and B3LYP results, respectively). A comparison between the ME, MAE, MRE, and MARE listed in table 3 for the complete set of systems and the corresponding entries for the non-metallic systems only (Si–LiF) shows that especially for the metallic systems (Na–Ag) the HF/DFT hybrids underperform with respect to the (conventional) PBE functional. This is clearly illustrated by figure 6 as well.

As discussed in [7], the inclusion of HF exchange in the hybrid functionals very likely causes an overestimation of the exchange splitting in d elements. The concomitant increase in the spin-polarization energy of the atomic system leads to an underestimation of the atomization energy of the d metals. Consequently, hybrid functionals fail to describe the d-metal atomization energies, whereas PBE works reasonably well.

This situation is even worse in the case of the B3LYP functional, for which the atomization energies of *all* metallic systems (Na–Ag in figure 6) are severely underestimated. Moreover, in the case of B3LYP this underbinding is present in all systems possessing substantial itinerant character, i.e., it affects the small- to medium-gap systems as well (Si–BN). Generally speaking, one may conclude that the more 'free-electron-like' the material is the larger the deviations of the B3LYP atomization energies to experiment are. Note that the materials in figure 6 are listed from left to right in order of increasing band gaps (e.g. E_g(Si) = 1.17 eV, E_g(GaAs) = 1.52 eV, etc). As shown in [8], the main reason for the poor performance of the B3LYP functional is the use of the LYP correlation energy: the LYP correlation functional does not attain the homogeneous electron gas (HEG) limit.

4.2.2. Heats of formation. Figure 7 shows the relative errors with respect to experiment, in the PBE, PBE0, HSE03, and B3LYP heats of formation for some representative *solid–gas* and *solid–solid* chemical reactions. As discussed in [8], the PBE calculations show a pronounced underestimation of the heats of formation (MARE(PBE) = 14% w.r.t. experiment), whereas the HF/DFT hybrids yield markedly better results (e.g. MARE(PBE0) = 8.8% and MARE(HSE03) = 9.5%). Most strikingly, however, the B3LYP description of the heats of formation is excellent (MARE(B3LYP) = 4.4%). The latter was judged most likely to be fortuitous [8]: B3LYP heats of formation are larger than the corresponding PBE, PBE0, HSE03 results, primarily because of its underestimation of the total energy of the metallic reactants. An overestimation of the total energy of the molecular reactant and underestimation of the energy of the metal in all likelihood cancels against a similar overestimation for the reaction product. All solid–gas reactions in figure 7 involve a metallic reactant and are thus subject to this line of reasoning. The only exception is the solid–solid SiC formation. This reaction does not involve a

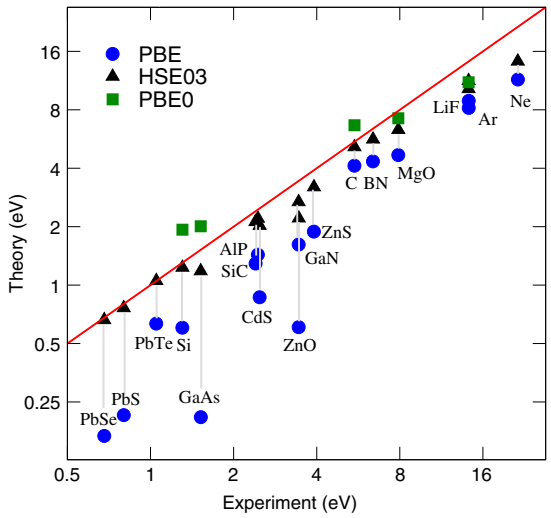

Figure 8. Band gaps from PBE, PBE0, and HSE03 calculations, plotted against data from experiment.

metallic reactant and, in line with the previous arguments, the B3LYP heat of formation for SiC is similar to that for PBE0 and HSE03.

4.3. Electronic properties

Figure 8 shows PBE, PBE0, and HSE03 band gaps plotted against data from experiment. As expected, the PBE calculations show the usual underestimation of the band gaps, which is typical for the conventional density functionals. The PBE0 and HSE03 hybrid functionals definitely provide an improved description of the band gaps compared to conventional DFT. In the case of HSE03, the improvements are most pronounced for small- to medium-gap systems [6, 7], whereas for large-gap systems (e.g. LiF, Ar, and Ne) the gaps are still underestimated. The PBE0 functional yields an overestimation of the band gaps in semiconductors, and similar to the HSE03 case an underestimation of the gaps in large-gap systems [7]. In large-gap systems, where the dielectric screening is very weak, the correct exchange term should approach the bare HF exchange, and admixing only 25% of HF exchange as is done in the PBE0 and HSE03 hybrids is not enough to correctly describe large-gap systems. Furthermore, as shown in [7], the PBE0 and HSE03 description of the electronic structure of metallic systems is not entirely satisfactory either: the HSE03 bandwidths are slightly, and the PBE0 bandwidths significantly, overestimated with respect to experiment. In metallic systems dielectric screening is strong, and one should ideally admix less than 25% of HF exchange to correctly describe the exchange interactions.

4.4. Transition metal monoxides

Table 4 lists the lattice constants a_0, local spin magnetic moments M_s, and band gaps Δ, for the transition metal monoxides (TMOs) MnO, FeO, CoO, and NiO, from LDA, HSE03, and B3LYP [24–26] calculations, as well as from experiment (see [27] and references therein).

Table 4. Lattice constants a_0 (Å), spin magnetic moments M_s (μ_B), and band gaps Δ (eV), for the transition metal monoxides MnO, FeO, CoO, and NiO, from LDA, HSE03, and B3LYP [24–26] calculations, as well as from experiment ([27] and references therein).

		LDA	HSE03	B3LYP	Expt.
MnO	a_0	4.31	4.44	4.50	4.45
	M_s	4.14	4.52	4.73	4.58
	Δ	0.4	2.8	3.92	3.9
FeO	a_0	4.17	4.33	4.37	4.33
	M_s	3.26	3.63		3.32/4.2
	Δ	0.0	2.2	3.70	2.4
CoO	a_0	4.10	4.26	4.32	4.25
	M_s	2.23	2.67	2.69	3.35/4.0
	Δ	0.0	3.4	3.63	2.5
NiO	a_0	4.06	4.18	4.23	4.17
	M_s	1.06	1.65	1.67	1.64
	Δ	0.4	4.2	4.10	4.0

As illustrated by table 4, conventional density functionals, e.g. the LDA, underestimate the TMO lattice constants and the local magnetic moments on the transition metal ions, and severely underestimate the TMO band gaps; FeO and CoO are even predicted to be metals. These discrepancies result from deficiencies of the LDA (or any other (semi-) local density functional) to describe the strongly localized transition metal 3d states: conventional density functionals yield 3d states that are spatially too delocalized.

The most widely used approaches to remedy this situation are the GW approximation, self-interaction corrections (SICs), the DFT + U method, and the use of HF/DFT hybrid functionals (see for instance [28] and references therein).

In general, the Hartree–Fock approximation tends to give rise to a higher degree of spatial localization of the wavefunctions than conventional density functionals, and this carries over to the HF/DFT hybrid functionals. As evident from table 4 the admixture of HF exchange in the hybrid functionals addresses the aforementioned deficiencies quite effectively. The HF/DFT hybrids yield larger lattice constants, local spin magnetic moments, and band gaps. In particular, the HSE03 functional gives TMO lattice constants and local spin magnetic moments that are in excellent agreement with experiment. The apparently large underestimation of the local magnetic moment in the case of CoO (and to a lesser extent FeO) stems from the neglect of spin–orbit coupling (SOC) in the calculations. The inclusion of SOC would give rise to an additional *orbital* magnetic moment.

Unfortunately, the agreement between the HSE03 and B3LYP TMO band gaps and experiment is still rather erratic, although they present a large improvement compared to the corresponding LDA results.

4.5. CO on d-metal surfaces

The failure of the conventional (semi-) local exchange–correlation density functionals to yield the correct adsorption site for CO on d-metal surfaces is well documented (see for instance [29]). Common density functionals predict CO to adsorb in the hollow sites of, e.g., Cu, Rh, and Pt, whereas

Table 5. The PBE, PBE0, and HSE03 adsorption energies (eV) of CO in the top and hollow (fcc and hcp) sites on the (111) surfaces of Cu, Rh, and Pt. For each surface and exchange–correlation functional the entry corresponding to the preferred adsorption site is underlined. All data taken from [30].

CO@	Site	PBE	PBE0	HSE03	Expt.
Cu(111)	top	0.709	<u>0.606</u>	<u>0.561</u>	0.46–0.52
	fcc	<u>0.874</u>	0.579	0.555	
	hcp	0.862	0.565	0.535	
Rh(111)	top	1.870	<u>2.109</u>	<u>2.012</u>	1.43–1.65
	fcc	1.906	2.024	1.913	
	hcp	<u>1.969</u>	2.104	1.996	
Pt(111)	top	1.659	1.941	1.793	1.43–1.71
	fcc	<u>1.816</u>	<u>1.997</u>	<u>1.862</u>	
	hcp	1.750	1.944	1.808	

experimentally it is found that CO adsorbs at the top site: as shown in table 5, the PBE functional incorrectly predicts CO to adsorb in the fcc-hollow site on Cu(111) and Pt(111), and in the hcp-hollow site on Rh(111) surfaces.

This probably results from an incorrect description of the position of the highest occupied molecular orbital (HOMO: 5σ) and the lowest unoccupied molecular orbital (LUMO: $2\pi^*$) of CO with respect to the Fermi energy of the metal (see [30] and references therein). Accordingly, the main motivation to study CO adsorption using HF/DFT hybrid functionals is the expected improvement in the description of the CO HOMO and LUMO.

Table 5 lists PBE0 and HSE03 adsorption energies for CO in the top and hollow (fcc and hcp) sites of Cu(111), Rh(111), and Pt(111) surfaces. A comprehensive analysis of HF/DFT hybrid calculations on CO adsorption energies is beyond the scope of this paper, and we will limit ourselves to restating the general conclusion drawn by Stroppa *et al* [30]:

(i) The admixture of HF exchange in the HF/DFT hybrid functionals reduces the tendency to stabilize adsorption at the hollow sites with respect to adsorption at the top site. The hybrid functionals yield an improved description of the position of the CO LUMO ($2\pi^*$) with respect to the Fermi level of the metal: the CO $2\pi^*$ is shifted upwards, away from the Fermi level. This reduces the CO $2\pi^* \leftrightarrow$ metal–d interaction (the 'backbonding' related to the partial occupation of the $2\pi^*$) and destabilizes adsorption in the hollow sites. Unfortunately, the aforementioned is counteracted by the fact that the HF/DFT hybrid functionals yield a too large metal–d band width. As shown in table 5, for the PBE0 and HSE03 functionals the net reduction in the CO $2\pi^* \leftrightarrow$ metal–d interaction is large enough to predict the right CO adsorption site on Cu(111) and Rh(111), but not on Pt(111), which has the largest metal–d band width. Also note that the HSE03 CO adsorption energies in the top and fcc-hollow sites on Cu(111) are almost degenerate, (the same for HSE03 and PBE0 adsorption energies in top and hcp sites on Rh(111)).

(ii) As illustrated by table 5, semilocal density functionals (such as the PBE functional) generally show a tendency to overestimate adsorption energies on metal surfaces [29]. Unfortunately, this seems to be the case for the PBE0 and HSE03 hybrid functionals as well. Even worse, for CO adsorption on Rh(111) and Pt(111), the PBE0 and HSE03 adsorption energies present a deterioration with respect to the PBE result.

5. Conclusions

This contribution presents an overview of the characteristics of the PBE0, HSE03, and B3LYP hybrid functionals applied to the description of the structural, thermochemical, and electronic properties of extended systems. In comparison to common (semi-) local density functionals, these may be summarized as follows:

(i) Compared to the PBE semilocal density functional, the PBE0 and HSE03 hybrid functionals yield an improved description of the structural properties (lattice constants and bulk moduli) of extended systems: a reduction of the overestimation of the lattice constants and the corresponding underestimation of the bulk moduli. The B3LYP hybrid functional performs slightly *worse* than the PBE functional, mostly (but not only) due to a poor description of the d metals.

(ii) The description of the atomization energies of extended systems is best at the PBE level. The PBE functional yields an overall underestimation of the atomization energies, that is further enhanced by the hybrid functionals. The latter underperform for metallic systems, in the case of the B3LYP functional even dramatically so. Worse still, the B3LYP underbinds all systems that possess substantial itinerant character, i.e. small- to medium-gap systems too. Excluding metals, the PBE0 and HSE03 hybrid functionals show a similar overall agreement with experiment as the PBE does.

(iii) For the calculation of heats of formation, the use of hybrid functionals presents a substantial improvement over the PBE semilocal density functional. Whereas the PBE shows a pronounced underestimation of the heats of formation, the hybrid functionals yield markedly better results. Most strikingly, the B3LYP description of the heats of formation, for the systems we considered, is excellent. This is believed to be fortuitous.

(iv) Compared to conventional density functionals, the PBE0 and HSE03 hybrid functionals provide a significantly improved description of the band gap in extended systems. The HSE03 band gaps for small- to medium-gap systems are in good agreement with experiment. For large-gap systems they still remain underestimated, but less so than with conventional density functionals. The PBE0 overestimates the band gap in semiconductors, and similar to the HSE03 underestimates the gap in large-gap systems. Both the PBE0 as well as the HSE03 functional overestimate the band widths in metallic systems.

(v) Conventional density functionals fail to correctly describe the structural and electronic properties of the transition metal monoxides: underestimation of the lattice constants, local magnetic moments, and band gaps (some transition metal monoxides are even incorrectly predicted to be metals). This originates from the fact that (semi-)

local density functionals yield 3d states that are spatially too delocalized. In keeping with what is generally known about the Hartree–Fock approximation, the hybrid functionals tend to give rise to a higher degree of spatial localization. This addresses all of the aforementioned deficiencies. In particular, the HSE03 yields transition metal monoxide lattice constants and local magnetic moments that are in excellent agreement with experiment.

(vi) Hybrid functionals present a modest improvement over conventional density functionals in the description of CO adsorption on d-metal surfaces: hybrid functionals reduce the tendency to stabilize adsorption at the hollow sites with respect to adsorption at the top site. Unfortunately, the results are by no means satisfactory. For several systems the hybrid functionals still yield the wrong site order and/or much too large adsorption energies (most notably CO@Pt(111)). This failure is related to the overestimation of the metal–d band widths (see (iv)).

In principle, the amount of HF exchange that should be admixed in a hybrid functional is system dependent and one should not expect that a fixed ratio of HF to density functional exchange will work well for all systems. In a broad generalization one might state that hybrid functionals perform well for molecules and insulators, but are lacking in the description of metallic systems. We are thus left with the problem of how to treat the aforementioned disparate systems on the same theoretical footing.

Acknowledgments

This work was supported by the Austrian *Fonds zur Förderung der wissenschaftlichen Forschung* within the START grant Y218.

References

[1] Curtiss L A, Raghavachari K, Redfern P C and Pople J A 1997 *J. Phys. Chem.* **106** 1063
[2] Ernzerhof M and Scuseria G E 1999 *J. Chem. Phys.* **110** 5029
[3] Adamo C and Barone V 1999 *J. Chem. Phys.* **110** 6158
[4] Paier J, Hirschl R, Marsman M and Kresse G 2005 *J. Chem. Phys.* **122** 234102
[5] Heyd J and Scuseria G E 2004 *J. Chem. Phys.* **121** 1187
[6] Heyd J, Peralta J E, Scuseria G E and Martin R L 2005 *J. Chem. Phys.* **123** 174101
[7] Paier J, Marsman M, Hummer K, Kresse G, Gerber I C and Ángyán J G 2006 *J. Chem. Phys.* **124** 154709
Paier J, Marsman M, Hummer K, Kresse G, Gerber I C and Ángyán J G 2006 *J. Chem. Phys.* **125** 249901 (erratum)
[8] Paier J, Marsman M and Kresse G 2007 *J. Chem. Phys.* **127** 024103
[9] Perdew J P, Burke K and Ernzerhof M 1996 *Phys. Rev. Lett.* **77** 3865
[10] Ernzerhof M 1996 *Chem. Phys. Lett.* **263** 499
[11] Ernzerhof M, Perdew J P and Burke K 1996 *Int. J. Quantum Chem.* **64** 285
[12] Perdew J P, Ernzerhof M and Burke K 1996 *J. Chem. Phys.* **105** 9982
[13] Heyd J, Scuseria G E and Ernzerhof M 2003 *J. Chem. Phys.* **118** 8207
Heyd J, Scuseria G E and Ernzerhof M 2006 *J. Chem. Phys.* **124** 219906 (erratum)
[14] Krukau A V, Vydrov O A, Izmaylov A F and Scuseria G E 2006 *J. Chem. Phys.* **125** 224106
[15] Frisch M J *et al* 2004 *GAUSSIAN 03, Revision C.02* (Wallingford, CT: Gaussian, Inc)
[16] GAUSSIAN Inc. 1994 *Gaussian NEWS* **5** 2
[17] Becke A D 1993 *J. Chem. Phys.* **98** 5648
[18] Becke A D 1988 *Phys. Rev.* A **38** 3098
[19] Vosko S H, Wilk L and Nusair M 1980 *Can. J. Phys.* **58** 1200
[20] Lee C, Yang W and Parr R 1988 *Phys. Rev.* B **37** 785
[21] Blöchl P E 1994 *Phys. Rev.* B **50** 17953
[22] Kresse G and Hafner J 1993 *Phys. Rev.* B **48** 13115
[23] Kresse G and Furthmüller J 1996 *Comput. Mater. Sci.* **6** 15
Kresse G and Furthmüller J 1996 *Phys. Rev.* B **54** 11169
[24] Alfredsson M, Price G D, Catlow C R A, Parker S C, Orlando R and Brodholt J P 2004 *Phys. Rev.* B **70** 165111
[25] Feng X-B and Harrison N M 2004 *Phys. Rev.* B **69** 035114
[26] Moreira I d P R, Illas F and Martin R L 2002 *Phys. Rev.* B **65** 155102
[27] Tran F, Blaha P, Schwarz K and Novák P 2006 *Phys. Rev.* B **74** 155108
[28] Franchini C, Bayer V, Podloucky R, Paier J and Kresse G 2005 *Phys. Rev.* B **72** 045132
[29] Feibelman P J, Hammer B, Nørskov J K, Wagner F, Scheffler M, Stumpf R, Watwe R and Dumesic J 2001 *J. Phys. Chem.* B **105** 4018
[30] Stroppa A, Termentzidis K, Paier J, Kresse G and Hafner J 2007 *Phys. Rev.* B **76** 195440